Online Supporting Information for

Visible light driven catalytic gold decorated Soft-Oxometalate (SOM) based nanomotors for organic pollutant remediation

Apabrita Mallick[a,b], Soumyajit Roy*[a,b]

[a]EFAML, College of Chemistry, Central China Normal University, 152 Luoyu Road, Wuhan, Hubei 430079, P. R. China. E-mail: s.roy@mail.ccnu.edu.cn

[b]EFAML, Materials Science Centre, Department of Chemical. Sciences, Mohanpur Campus, Indian Institute of Science Education & Research, Kolkata, 741246 West Bengal. E-mail: s.roy@iiserkol.ac.in

Supporting Videos

SI Video 1: Motion of TiO_2-{Mo_7}-Au nanomotors at different light intensities.

SI Video 2: 'On-Off" Motion of TiO_2-{Mo_7}-Au nanomotors under $5X10^3$ Lux of light.

SI Video 3: Motion of TiO_2-{Mo_7}-Au nanomotors under $30X10^3$ Lux of light in different concentrations of NaCl.

SI Video 4: Motion of TiO_2-{Mo_7}-Au nanomotors under $30X10^3$ Lux of light after different time intervals.

Characterization of the TiO_2-{Mo_7}-Au nanomotors:

A. Electron Absorption Spectroscopy (EAS) and Photoluminescence (PL) studies:

EAS illustrates that TiO_2 has a peak at 283 nm and {Mo_7} exhibits absorption maxima at 211 nm which match well with the literature.[1] For TiO_2-{Mo_7} this maxima shows a bathochromic shift to 220 nm which implies binding of {Mo_7} to the TiO_2 surface and this is further red-shifted to 236 nm in TiO_2-{Mo_7}-Au. The band due to TiO_2 is also red shifted to 320 nm and the absorbance is more in this case. Also, surface plasmon resonance (SPR) arises in the spectrum in the form of a band (given in zoomed inset of Figure 1C) at 545 nm as the ramification of formation of gold nanoparticles embedded on the surface of TiO_2-{Mo_7}. The SPR peak is not very prominent which nullifies the presence of free Au nanoparticles in the dispersion. PL studies (Figure 1D) also compliment the above results. In anatase TiO_2 photoluminescence results from at least two trap-state distributions and radiative recombinations of electrons and holes. Surface defects on TiO_2 are bound to interact with the {Mo_7} and Au present on the surface of TiO_2 as they can exchange electrons with the semiconductor. This explains why the energy corresponding to emission decreases in TiO_2-{Mo_7} and further in TiO_2-{Mo_7}-Au. TiO_2 is an indirect band gap material and constructing the Tauc plot from EAS its band gap is found to be 3.19 eV which matches with the literature value and proves that it is photoactive in UV range. With incorporation of {Mo_7} and Au the band gap reduces to 2.67 eV (corresponding to 464 nm) thus fulfilling our necessary requirement to make it photoactive in visible light. The E_g value is substantially reduced by 0.52 eV from TiO_2 to TiO_2-{Mo_7}-Au. {Mo_7} acts as electron scavenger and decrease the rate of charge recombination in TiO_2 changing the interfacial electron transfer and reducing E_g by 0.25 eV and Au directly affects the Schottky barrier height at the interface by exchange of electrons with TiO_2 which further reduces the band gap to 2.67 eV.

B. Scanning electron microscopy (SEM), Transmission electron microscopy (TEM) and Dynamic Light Scattering (DLS) studies:

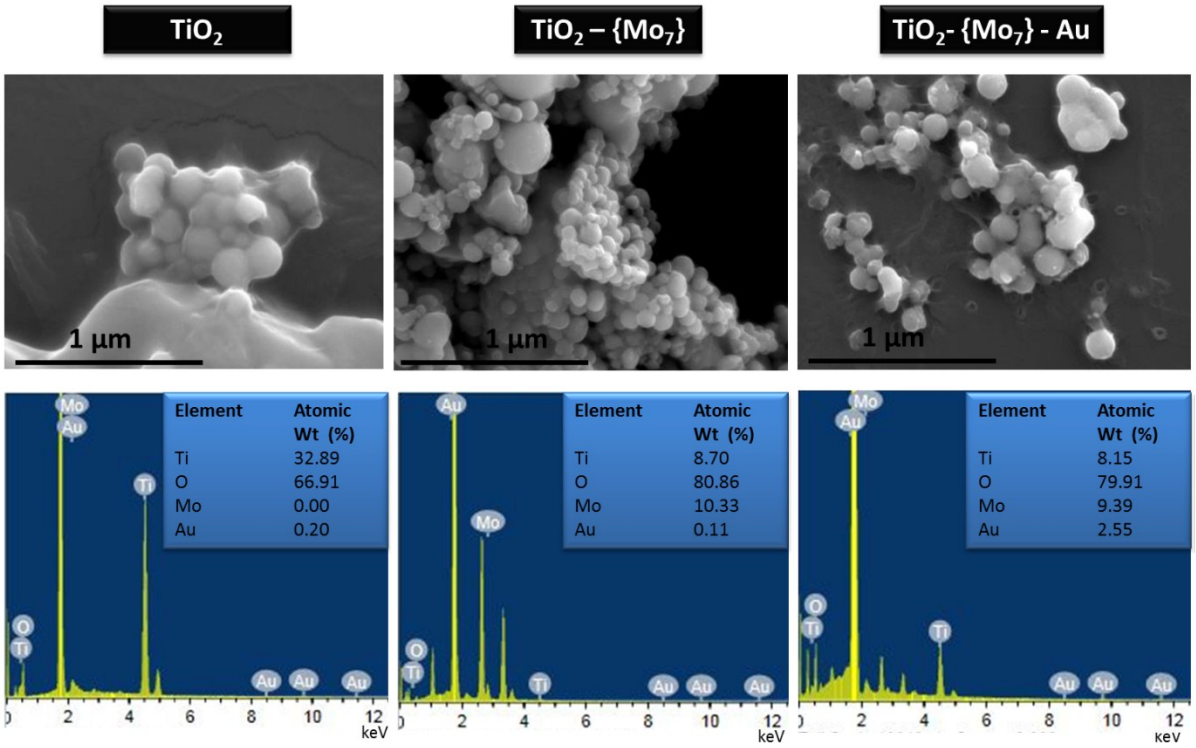

Figure S1: SEM-EDS analysis of TiO_2, TiO_2-{Mo_7} and TiO_2-{Mo_7}-Au showing atomic weight % of constituent elements Ti, O, Mo and Au

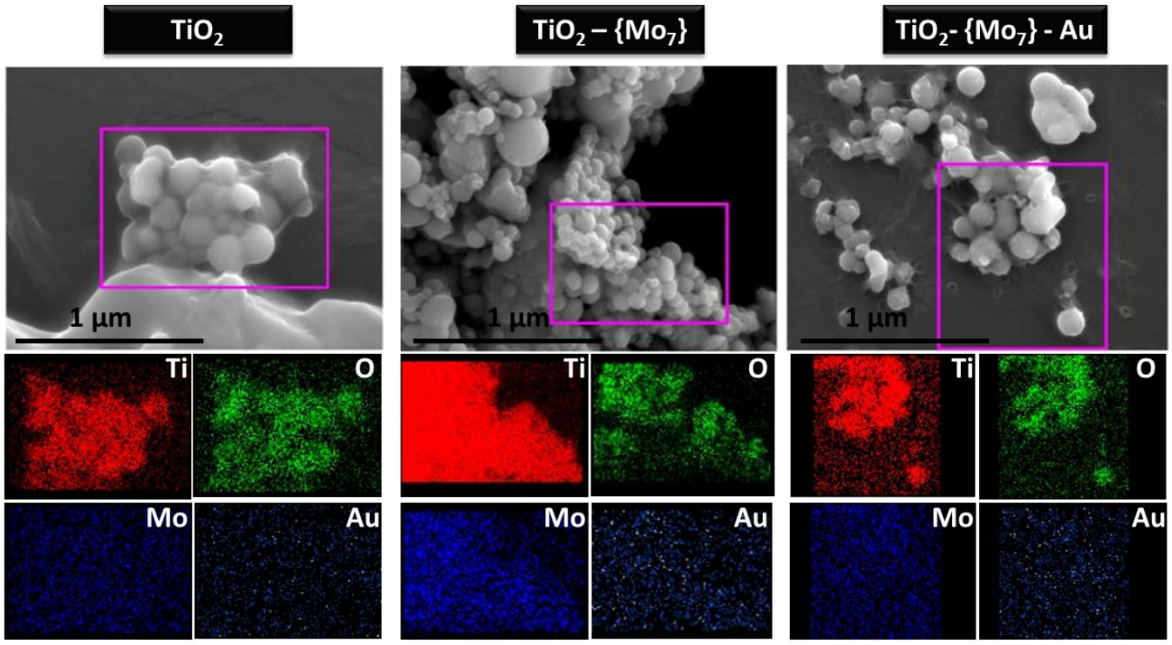

Figure S2: SEM-EDS mapping of TiO_2, TiO_2-{Mo_7} and TiO_2-{Mo_7}-Au showing distribution of constituent elements Ti, O, Mo and Au

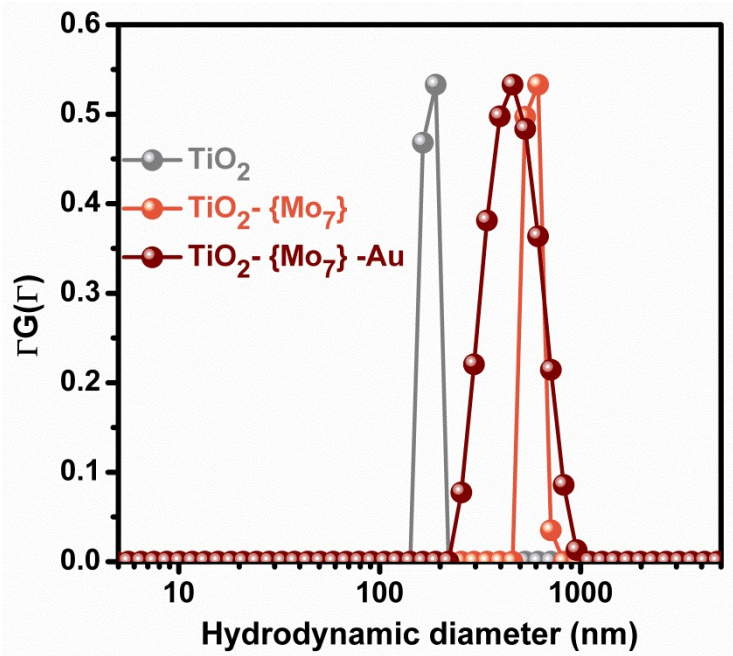

Figure S3: Dynamic Light Scattering study of TiO_2, TiO_2-{Mo_7} and TiO_2-{Mo_7}-Au dispersions in water.

From DLS data and SEM and TEM images it is evident that TiO_2 has a spherical or globular structure with size ranging between 140-230 nm and its aqueous dispersion has moderate stability (ζ-potential = -33.1 mV). Modification with $\{Mo_7\}$ does not change the topology but leads to agglomeration of TiO_2 particles with a surface coating of $\{Mo_7\}$ as $\{Mo_7\}$ are prone to self-assembly in aqueous dispersions due to charge regulation and hydrogen bonding. The hydrodynamic diameter of these agglomerated particles is widely distributed ranging from 220 nm to 990 nm and have incipient stability (-27.2 mV). EDS mapping shows the distribution of $\{Mo_7\}$ bound to TiO_2. Further reaction of TiO_2-$\{Mo_7\}$ with $AuCl_4^-$ results in well dispersed Au nanoparticles on the surface of TiO_2-$\{Mo_7\}$ with size 450-750 nm which is confirmed from EDS mapping. TEM micrograph (Figure S4 D and E) shows formation of 700 nm sized TiO_2-$\{Mo_7\}$-Au particles with 10 nm Au nanoparticles spread on the surface.

The high resolution TEM (HR-TEM) and corresponding Fast Fourier Transform (FFT) pattern (Figure S4 E and F) reveals the formation of 10 nm sized Au nanoparticles which are crystalline in nature with (200) and (111) crystalline facets of Au in fcc phase with well-defined interplanar spacing of d = 1.9 Å and d = 2.2 Å respectively. HAADF-STEM image (Figure S4 G and H) has strong image contrast at certain places which clearly reveals the presence of Au nanoparticles appearing as bright spots. This is due to the fact that in high-angle annular dark field mode, the intensity of the STEM images strongly depends on the atomic number, Z and since Au has the highest Z amongst all other constituent atoms in TiO_2-$\{Mo_7\}$-Au they appear as bright spots in Figure S4 H.

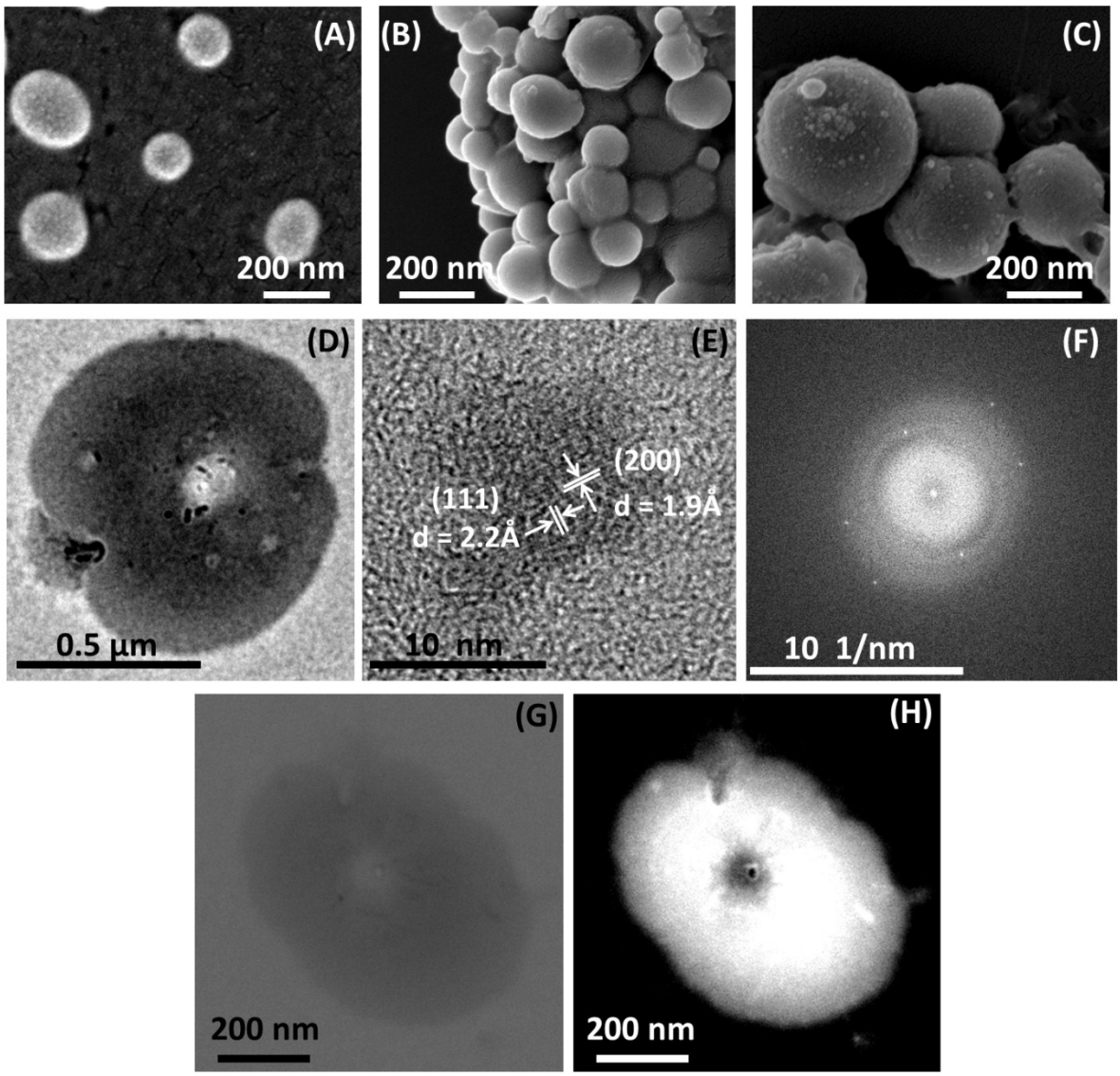

Figure S4: Scanning Electron Microscopy (SEM) images of (A) TiO_2, (B) TiO_2-{Mo_7} and (C) TiO_2-{Mo_7}-Au. HR-TEM images of (D) TiO_2-{Mo_7}-Au and (E) Au nanoparticle on the surface of TiO_2-{Mo_7} showing the crystalline facets and interplanar distances. (F) FFT image of the Au nanoparticle from which interplanar distances are calculated. (G) and (H) represent the STEM-HAADF images of TiO_2-{Mo_7}-Au.

C. Powder X-Ray Diffraction (PXRD) studies:

The crystalline nature of the particles can further be proved from powder X-Ray diffraction (PXRD). From Figure S5, anatase TiO_2 shows prominent peaks corresponding to (101), (004), (200), (105), (211) and (204) faces. In TiO_2-{Mo_7}, no significant peak due to {Mo_7} is observed. This may be ascribed to formation of a very thin layer of {Mo_7} on the surface of

TiO_2 and thus the peaks of TiO_2 only become prominent. This can also be argued from the TEM-EDS spectrum and mapping where very low % of Mo is observed as compared to Ti. For TiO_2-{Mo_7}-Au an additional peak arises at 44.3^0 which may be assigned as (200) plane of fcc lattice of Au. From HR-TEM images of Au nanoparticles we have seen existence of two planes (111) and (200) and also from the image (111) plane is more prominent. So naturally we should expect a peak for (111) plane in PXRD. But in accordance with literature, the peak due to (111) plane should appear at 39^0 [2] which is shrouded by an intense peak corresponding to (004) plane of TiO_2.

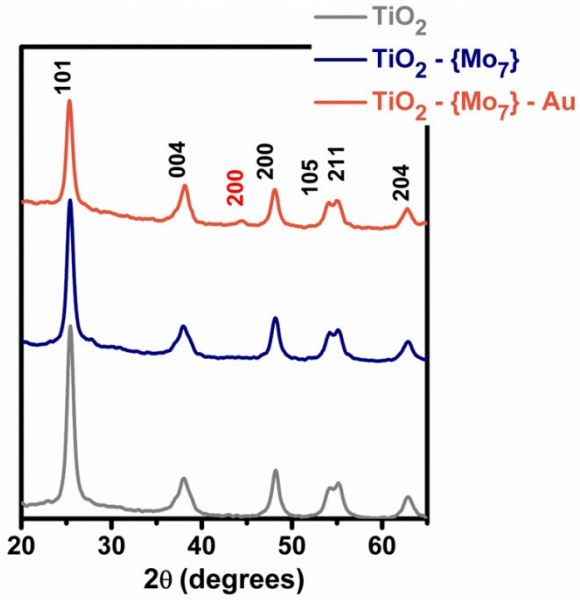

Figure S5: Powder X-Ray Diffraction (PXRD) patterns of of TiO_2, TiO_2-{Mo_7} and TiO_2-{Mo_7}-Au. The peak corresponding to (200) plane of Au nanoparticles is denoted with red colour.

D. Fourier-Transform Infra-Red (FT-IR) and Raman spectroscopic studies:

FT-IR and Raman spectroscopic studies (Figure S6 A and B) also confirm the formation of thin layer of {Mo_7} on TiO_2 though FT-IR cannot provide any insight to the formation of TiO_2-{Mo_7}-Au, unlike Raman. The vibrational bands of {Mo_7} are not prominent in TiO_2-{Mo_7} from FT-IR as well as Raman. But in case of Raman spectrum of TiO_2-{Mo_7}-Au one

vibrational band at 890 cm^{-1} corresponding to Mo=O stretching is observed, which has shifted due to the interaction of $Mo=O_t$ with Ti-O. The four bands of TiO_2 (141.3, 393.1, 511.2, 635.5) also manifest shifts by few nanometers due to interaction with $\{Mo_7\}$ and Au.

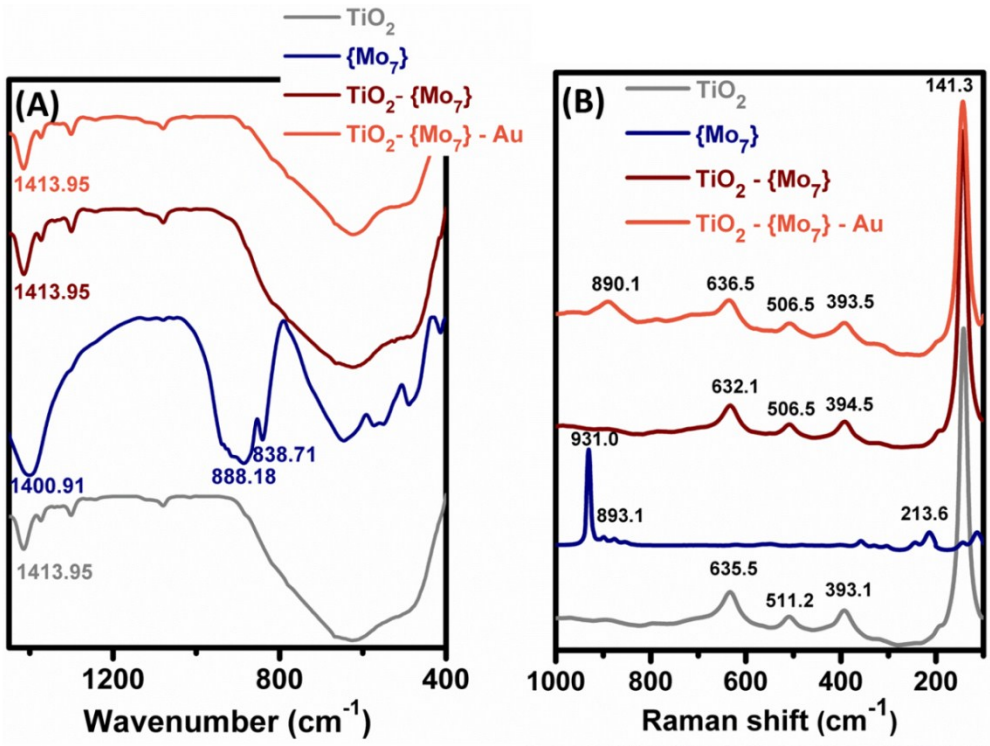

Figure S6: (A) Fourier-Transform Infra-Red spectra and (B) Micro Raman spectra of TiO_2, $\{Mo_7\}$, TiO_2-$\{Mo_7\}$ and TiO_2-$\{Mo_7\}$-Au.

Band gap and band structure of TiO_2, $\{Mo_7\}$, TiO_2-$\{Mo_7\}$ and TiO_2-$\{Mo_7\}$-Au:

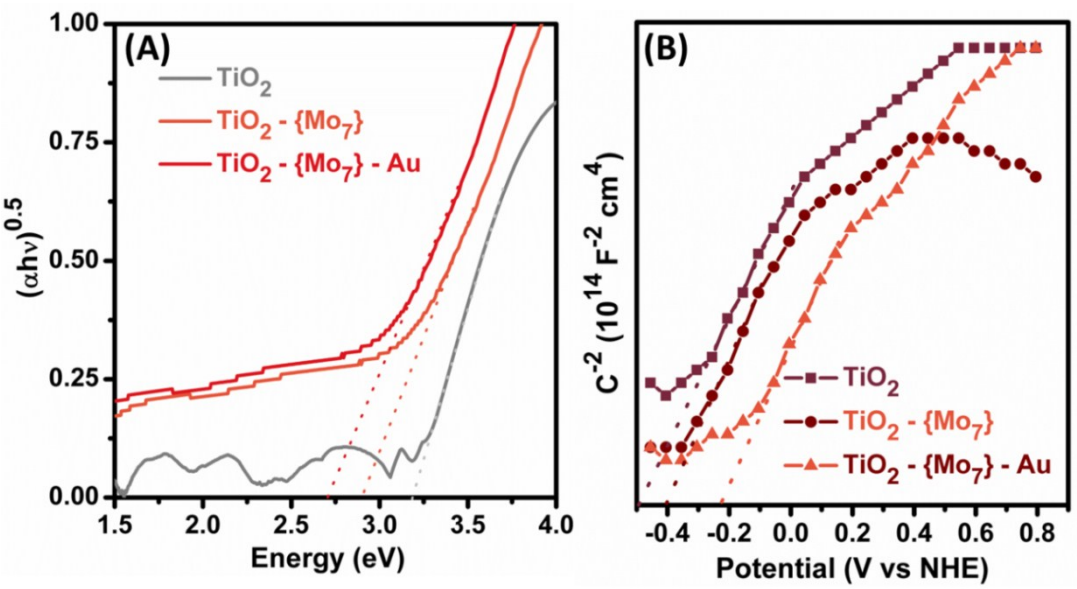

Figure S7: (A) Tauc plot generated from EAS studies of TiO_2, TiO_2-$\{Mo_7\}$ and TiO_2-$\{Mo_7\}$-Au. (B) Mott-Schottky plot generated from electrochemical experiments of TiO_2, TiO_2-$\{Mo_7\}$ and TiO_2-$\{Mo_7\}$-Au

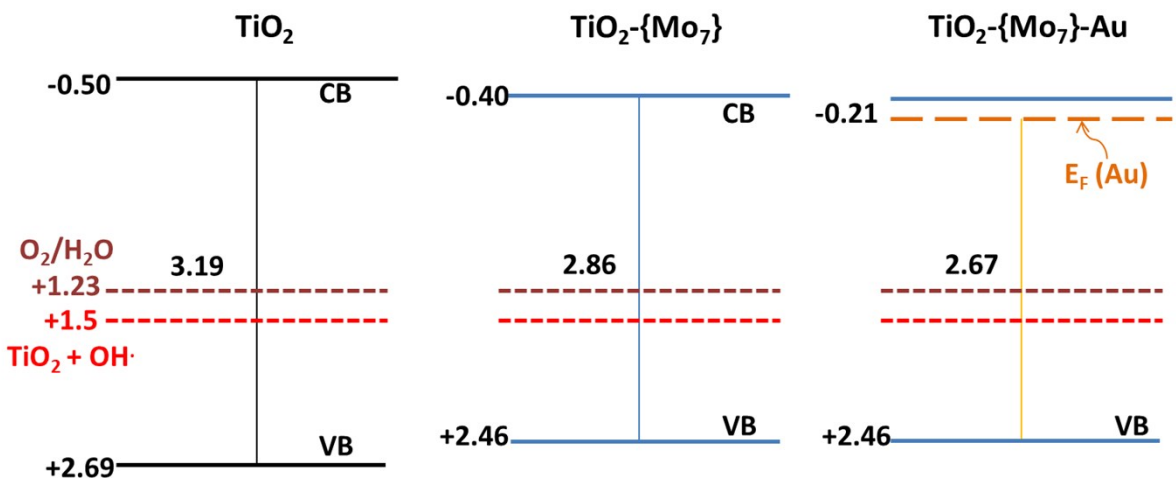

Figure S8: Schematic representation of band structure of TiO_2, TiO_2-$\{Mo_7\}$ and TiO_2-$\{Mo_7\}$-Au along with redox potentials of O_2/H_2O and [TiO_2 + $OH^{\cdot}$].

Motion of the nanomotors in presence of NaCl and after different time intervals of light exposure:

A. Effect of salt, NaCl on the motion of the nanomotors:

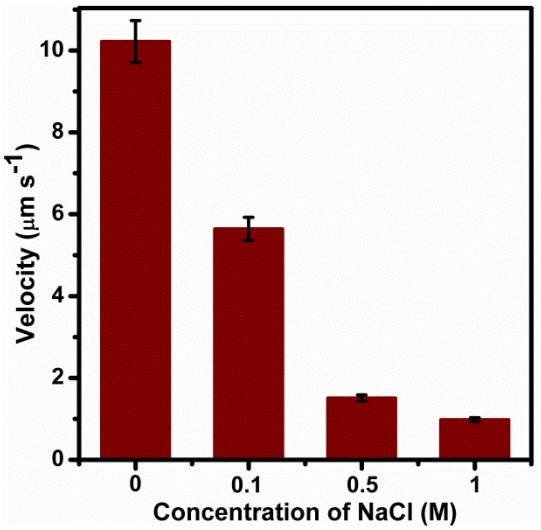

Figure S9: Velocity of the TiO_2-{Mo_7}-Au nanomotors with and without presence of NaCl at light intensity 30000 Lux. With increasing NaCl concentration the velocity decreases.

B. Effect of time of light exposure on the motion of the nanomotors:

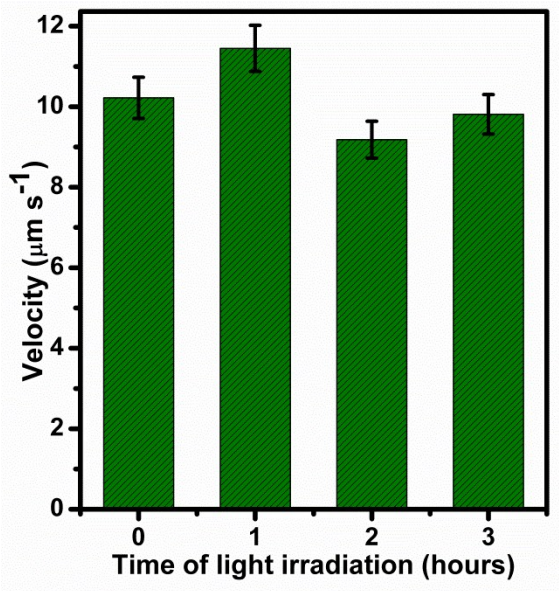

Figure S10: Velocity of the TiO_2-{Mo_7}-Au nanomotors observed on exposure to 30000Lux light at time intervals of 0 (initial), 1, 2 and 3 hours. They are almost similar confirming the nanomotor has a lifetime of at least 3 hours.

Mass spectra of benzyl bromide, benzyl alcohol and benzaldehyde from GC-MS:

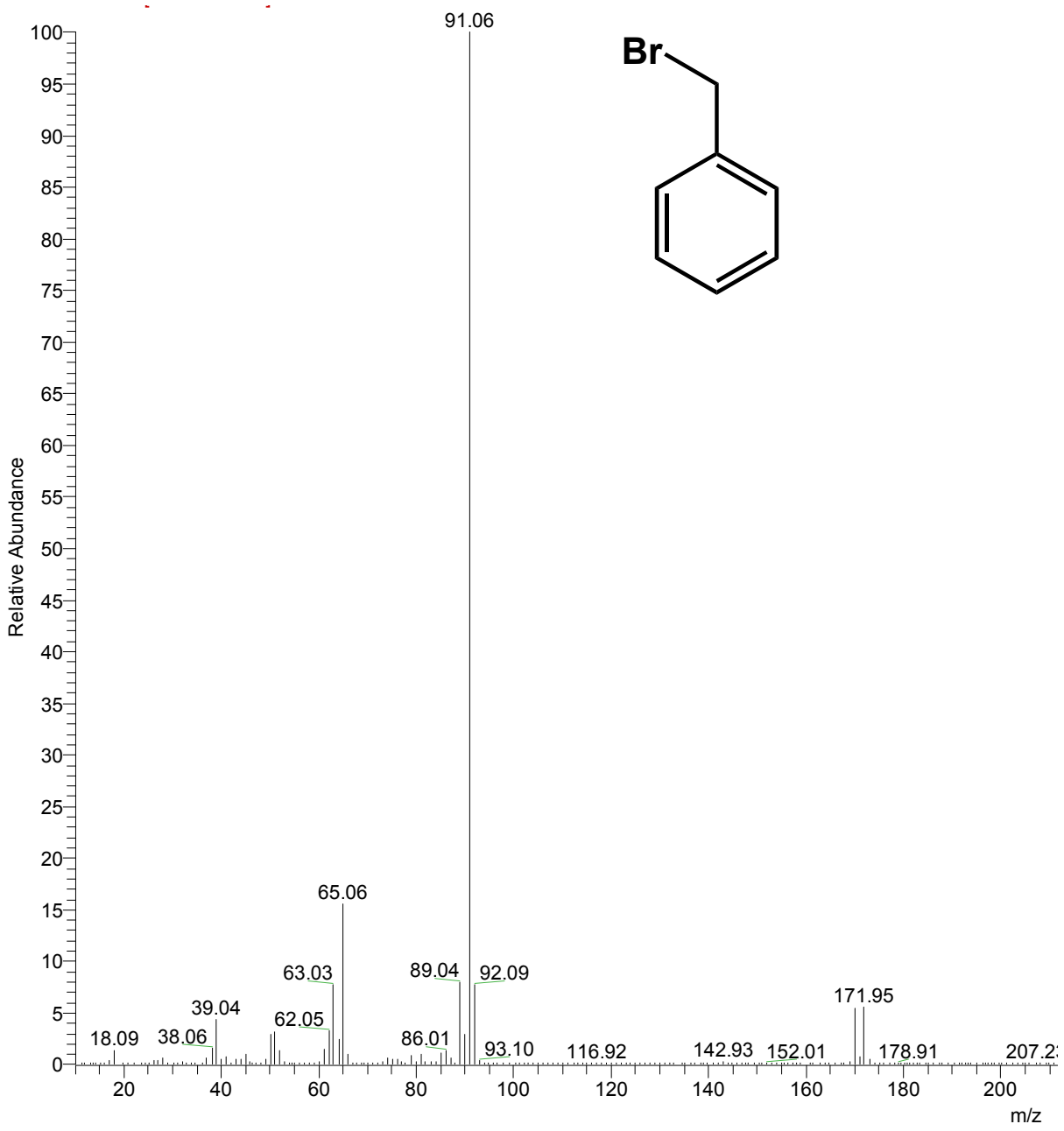

Figure S11: Mass spectrum of benzyl bromide generated from GC-MS

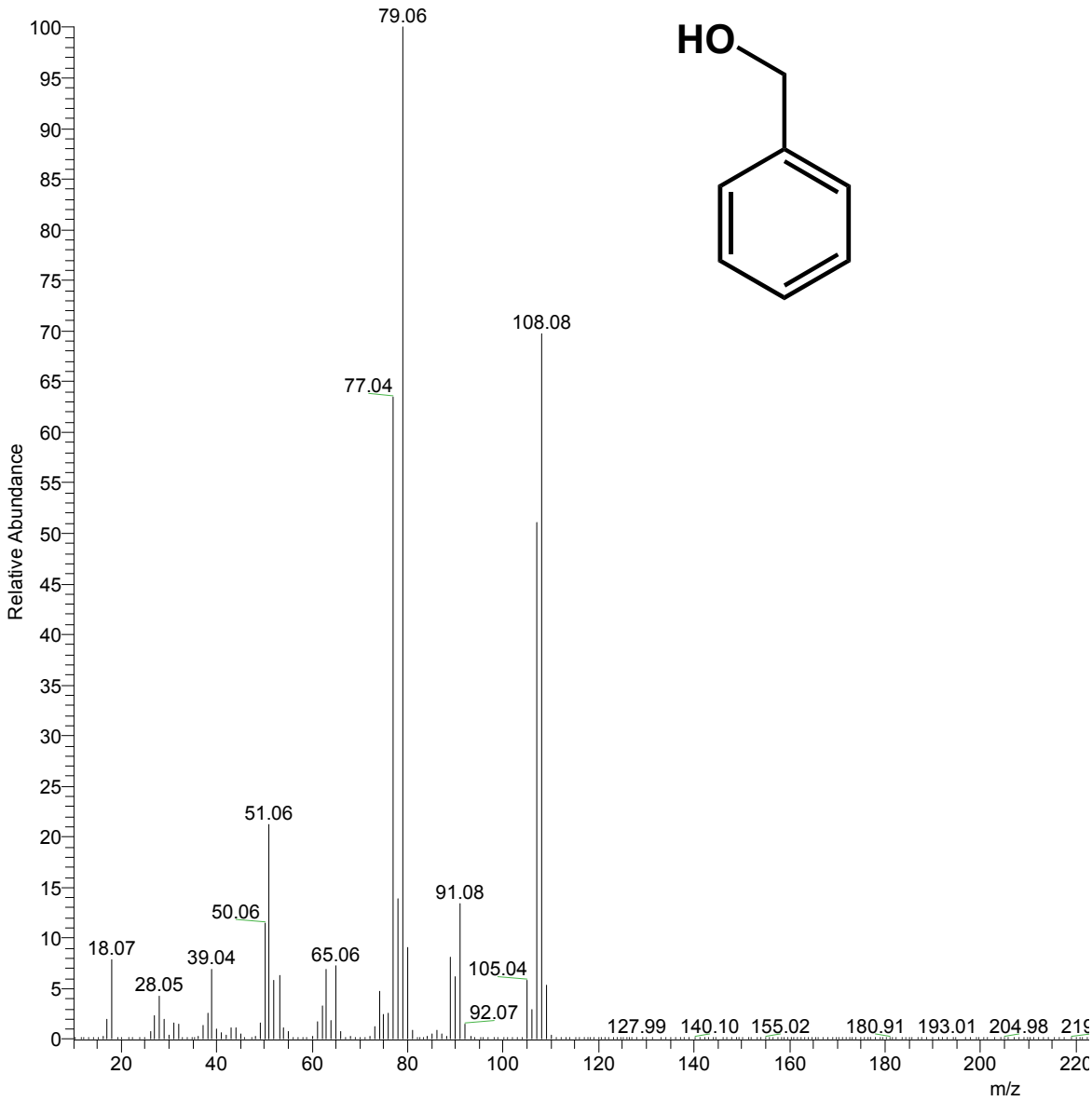

Figure S12: Mass spectrum of benzyl alcohol generated from GC-MS

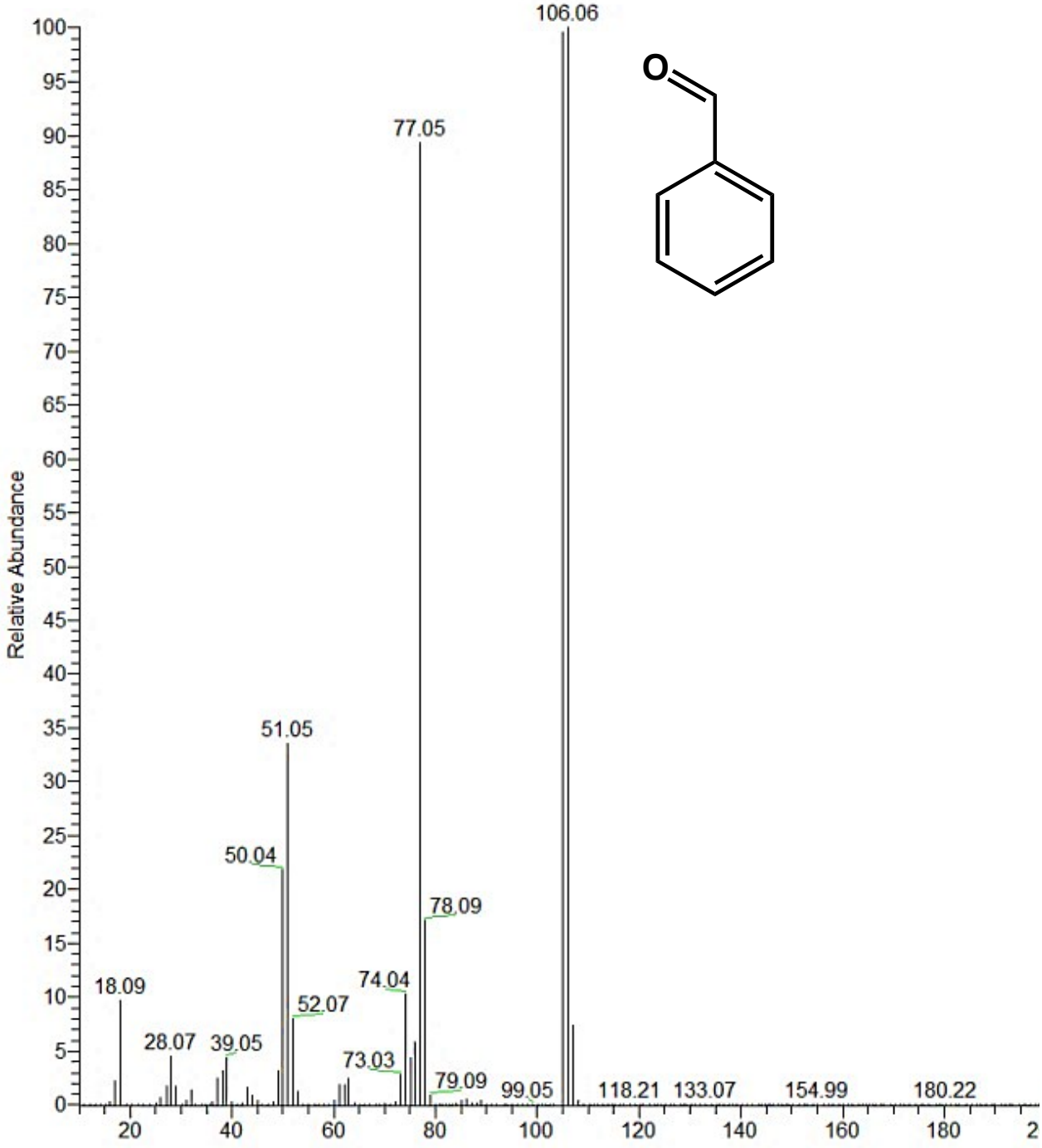

Figure S13: Mass spectrum of benzaldehyde generated from GC-MS

References:

1. S. Das, P. Thomas and S. Roy, *Eur. J. Inorg. Chem.*, 2014, **2014**, 4551-4557.
2. G. Zhang, Y. Wang, X. Wang, Y. Chen, Y. Zhou, Y. Tang, L. Lu, J. Bao and T. Lu, *Appl. Catal., B*, 2011, **102**, 614-619.